



Supercontinuum spectra above 2700 nm in circular lattice photonic crystal fiber infiltrated chloroform with the low peak power

Thuy Nguyen Thi¹ · Lanh Chu Van²

Received: 8 March 2023 / Accepted: 26 June 2023

© The Author(s), under exclusive licence to Springer Science+Business Media, LLC, part of Springer Nature 2023

Abstract

The broad supercontinuum spectrum in chloroform infiltrate hollow-core circular photonic crystal fibers with low peak powers of 1.44 kW and 20 kW has been investigated. The improvement in optical properties of the photonic crystal fibers is attributed to the difference air holes's size of the rings in the cladding, where the air holes's size in the first ring are smaller than others, and the infiltration of chloroform to the core. The flat dispersion, small effective mode area of $1.43 \mu\text{m}^2$, low confinement loss of 2.47 dB/m at $0.945 \mu\text{m}$ pump wavelength is responsible for the broad supercontinuum spectra of 753.9 nm in the first fiber with all-normal dispersion. The soliton dynamics provides bandwidth up to 2779.6 nm at a pump wavelength of $1.4 \mu\text{m}$ through supercontinuum generation in the second fiber with anomalous dispersion. The results further demonstrate that it is possible to generate broad supercontinuum spectra in the specified wavelength region thanks to exact control of photonic crystal fibers dispersion properties by using suitable highly nonlinear fluids and changing the air hole's size in the innermost ring of the photonic crystal fibers.

Keywords Photonic crystal fibers · Chloroform · Flat dispersion · Small effective mode area · Broad supercontinuum spectra

1 Introduction

Supercontinuum (SC) generation is a process where an extremely short pulse of high intensity, e.g., laser light propagating through a strong nonlinear medium, causes a continuous expansion of the output pulse over a broad wavelength range [1]. Recently, using a nonlinear medium such as a photonic crystal fiber (PCF) to generate SC has been an interesting topic attracting the attention of many research groups worldwide. Because of design flexibility, PCF can be usually made with tailored chromatic dispersion properties. Furthermore, it also often exhibits increased nonlinearity due to the strong mode confinement. Selecting a variety of geometries, creating structural defects, or filling air holes with highly nonlinear liquids are common ways to optimize

the optical properties of PCF helping to obtain broader SC spectra.

The unusual dispersion characteristics of PCFs are mainly responsible for the strong nonlinear interactions over a fiber length. In SC generation, these interactions are demonstrated through several nonlinear effects including soliton fission, four-wave mixing (FWM), self-phase modulation (SPM), soliton fission (SF), soliton self-frequency shift (SSFS), stimulated Raman scattering, etc., [1]. Suppose the pump wavelength is chosen at a value greater than the zero dispersion wavelength (ZDW), i.e., under anomalous dispersion regime pumping conditions. In that case, the spectrum will be greatly broadened due to the main domination of the soliton dynamics. But modulation instability can be found; as a result, the input pulse can be noise amplified and the SC light is incoherent [2–4]. To enhance the coherence of the spectrum in SC generation, many researchers have focused on PCFs with all-normal dispersion (ANDi). The self-phase modulation (SPM) and optical wave breaking (OWB) induce four-wave mixing (FWM) helps to achieve a broad SC spectrum when the PCF is excited by a femtosecond laser in ANDi regime [5–7]. Since there is no soliton formation, the spectrum is quite flat and a single pulse is maintained

✉ Lanh Chu Van
chuvanlanh@vinhuni.edu.vn

¹ University of Education, Hue University, 34 Le Loi, Hue City, Vietnam

² Department of Physics, Vinh University, 182 Le Duan, Vinh City, Vietnam

in the time domain. With outstanding features such as large bandwidth, high power density and good coherence, SC is of great significance in application including optical coherence tomography, fluorescence microscopy, optical telecommunication systems, gas sensing, biomedical imaging, etc. [8–13].

With the rapid development of fiber optic technology, new PCF materials or hybrid materials with many outstanding properties have always been the target of researchers despite many recent reports on liquid-core PCF (L-PCF). Liquids have good propagation characteristics from the visible to near-infrared spectral region and high nonlinear refractive indices of n_2 (two orders of magnitude larger than that of pure silica), which makes L-PCF confirmed as an ideal nonlinear medium for increasing the efficiency of SC. The characteristic quantities including chromatic dispersion, nonlinear coefficient, effective mode area and confinement loss are changed markedly when PCF is infiltrated with nitrobenzene [14–16], carbon tetrachloride [6, 7, 17], tetrachlorethylene [4, 18], toluene [5, 19–21], carbon disulfide [3, 22–24], benzene [2, 25]. In experiments, the works [5, 6, 17, 23] have shown that L-PCFs are fabricated by the conventional stack-and-draw method. Liquids are filled into the core by integrating a microfluidic pump system using a thermal fusion splicer or laser writing technique [26]. Along with this, L-PCF presents advantages in the application of temperature sensing, interferometer with high sensitivity, photon-pair generation, and optical wavelength conversion [27–29].

Until now, there have been very few publications on SC generation using chloroform-filled hollow-core PCF and these results are mainly reported by numerical simulation despite the fact that chloroform is a liquid with many interesting properties. First, its linear refractive index is only about 0.012 lower than that of silica [30], which will further improve the coupling efficiency with the standard silica fibers used in the all-fiber pump laser system. Second, its nonlinearity ($n_2 = 1.64 \times 10^{-19} \text{ m}^2 \cdot \text{W}^{-1}$) [31] is one order of magnitude higher than that of fused silica ($n_2 = 2.74 \times 10^{-20} \text{ m}^2 \cdot \text{W}^{-1}$) but similar to toluene ($n_2 = 16 \times 10^{-19} \text{ m}^2 \cdot \text{W}^{-1}$) and carbon tetrachloride ($1.53 \times 10^{-19} \text{ m}^2 \cdot \text{W}^{-1}$) [32], allowing light to be confined better in the core of the PCF. Third, its toxicity is not significant when compared with carbon disulfide and toluene [33] because the toxicity of liquids is essential when considering safety in the practical application of PCF. A laser pulse with 2 kW low peak power excited at 0.8 μm , propagating in a PCF in the anomalous dispersion regime provides a broad spectrum of 1100 nm [34]. This work also presented dispersion of PCF infiltrated chloroform is flatter than carbon disulfide, resulting in a broader SC spectrum. The SC spectrum of 1020 nm was obtained using PCF with ANDi has small values in the -20 to -50 ps/nm.km despite the rather large peak power of 47 kW [35].

With a small peak power of 2.5 kW, the two optimized fibers with ANDi and anomalous dispersion in [36] also generated SC with a broad spectrum of 660 nm and 800 nm, respectively. In addition, the AsSe₂-suspended core fiber with three air holes was filled with chloroform and demonstrated the ability to broaden the SC spectrum from 1 to 14 μm using short pulses with 10 kW peak power and 50 fs pulse duration at 2560 nm [37]. Furthermore, efficient pulse compression using chloroform-filled PCF was also reported in [38, 39]. In these works, PCF with hexagonal lattice or suspended core was observed. Similarly, the hexagonal lattice PCF with air holes permeated with chloroform, was investigated “to nullify the deleterious effects of temperature fluctuations on continuum width and soliton pulse propagation” [40]. Finally, to our knowledge, there is no experimental evidence yet to investigate SC spectral expansion based on chloroform-infiltrated PCFs. However, by experimentally, some other works verified a markedly improved SC generation efficiency using other liquids-infiltrated PCFs with high nonlinearity similar to chloroform. SC spectra spanning 950–1100 nm with 10 nJ input pulse energy at 1030 nm based on toluene-infiltrated PCFs with all-normal dispersion was reported in the work [5]. The publication [6] demonstrated the generation of an all-normal dispersion supercontinuum in the 850–1250 nm wavelength range using an available 1030 nm fiber laser with 400 fs and 25 nJ input pulses via carbon tetrachloride-filled PCFs. An octave-spanning SC in the range 1.1–2.7 μm at 14 nJ pulse energy with capillary fiber infiltrated with CS₂ pumped in the anomalous dispersion regime by a 460 fs laser operating at 1.95 μm [41]. An octave-spanning SC bandwidth (1.1 μm to 2.4 μm) using a core of C₂Cl₄-filled PCF was presented in the paper [42]. Input pulse has energy as low as 0.5 nJ with 270 fs duration at 1.92 μm . Most recently, a water-filled-cladding PCF generated the flat spectral SC with a bandwidth of 102.5 nm at 1030 nm wavelength with input energy of 9.0 nJ and pulse duration of 400 fs [43]. Therefore, the results of SC studies using chloroform-infiltrated PCFs by simulation will provide reliable evidences to verify the efficacy in further experimental studies. Table 1 summarizes some results of SC studies using chloroform-infiltrated silica-based PCF and different liquids based on numerical simulation.

In this paper, we demonstrate the ability to improve dispersion and nonlinear properties of chloroform-infiltrated PCF to generate broad-spectrum SC above 2700 nm based on numerical simulation. The PCFs are designed with a circular lattice to meet the requirement of tight light confinement in the core due to the circular lattice's higher symmetry than other lattices. The defects are introduced into the lattice structure by reducing the size of the air holes of the first ring around the core. Together with the infiltrating of chloroform into the hollow core of PCFs, their optical properties are significantly improved to enhance SC spectral expansion

Table 1 Overview SC generation in several chloroform and different liquids-infiltrated silica-based PCFs

Structures	Liquids	Fiber length (cm)	Pump wavelength (μm)	Dispersion regime	SC range (nm)	Input peak power (kW)	Refs.,
Hexagonal	Chloroform	0.5	0.8	Anomalous	1100	2	[34]
Hexagonal	Chloroform	1	1.06	Anomalous	1020	47	[35]
Hexagonal (#F ₁)	Chloroform	10	0.92	All-normal	660	2.5	[36]
Hexagonal (#F ₂)		10	1.03	Anomalous	800	2.5	
Hexagonal (#F ₁)	Nitrobenzene	5	1.03	Anomalous	1400	0.83	[16]
Hexagonal (#F ₂)		5	1.56	All-normal	1300	5.56	
Hexagonal (#F ₃)		5	1.56	Anomalous	1000	0.67	
Hexagonal (#F ₁)	Carbon tetrachloride	30	1.35	Anomalous	About 1400	2.67	[13]
Hexagonal (#F ₂)		30	1.064	All-normal	About 400	2.67	
Hexagonal (#F ₁)	Tetrachlorethylene	5	1.56	All-normal	1200	16.67	[18]
Hexagonal (#F ₂)		10	1.56	Anomalous	1000	16.67	
Hexagonal (#F ₃)		10	1.03	Anomalous	1700	20.83	
Circular (#F ₁)	Toluene	1	1.064	All-normal	950	0.45	[20]
Circular (#F ₂)		10	1.55	Anomalous	2386	0.56	
Hexagonal (#I _{0.3})	Toluene	10	1.55	All-normal	650	7.14	[19]
Hexagonal (#I _{0.35})		10	1.55	Anomalous	750	6.67	
Hexagonal	Carbon disulfide	14	1.56	Anomalous	640	560	[24]
Hexagonal (#F ₁)	Benzene	1	1.55	All-normal	1300	55	[25]
Hexagonal (#F ₂)		1	1.55	Anomalous	2000	37	
Hexagonal (#F ₃)		1	1.55	Anomalous	2900	37	

efficiency. Based on a detailed analysis of numerical simulation results, two fibers with flat all-normal and anomalous dispersion with low dispersion values of -1.629 ps/nm.km and 2.619 ps/nm.km, respectively, and small effective mode area are selected as SC generation nonlinear medium. The pulse is injected at 0.945 μm wavelength with 0.13 nJ energy and 90 fs duration (corresponding to 1.44 kW peak power) broadened from 596.1 to 1350 nm when propagating in 10 cm of the first fiber length. With a pump wavelength of 1.4 μm in an anomalous dispersion regime, the second fiber generates SC with a spectrum ranging from 750.4 nm to 3530 nm with an input pulse of 0.9 nJ of 45 fs duration (peak power of 20 kW).

This paper is organized into four sections. In the first section, an overview of SC studies using highly nonlinear liquid infiltrated-PCF are presented in detail. Section 2 describes the structure of PCF with corresponding lattice parameters. In Sect. 3, the chromatic dispersion of chloroform-infiltrated PCF are discussed in detail based on numerical simulation results. More, the characteristic quantities such as effective mode area, nonlinear coefficient and confinement loss and structural parameters of two proposed fibers for SC are also introduced in this section. Section 4 simulates numerically how the low peak power input pulses are broadened after propagating in the fiber by solving the generalized nonlinear Schrödinger equation, where the influence of the main nonlinear effects and fiber parameters on the bandwidth and

flatness are also covered. Finally, some conclusions about the SC generation efficiency of chloroform-infiltrated PCFs compared with some other publications are shown.

2 Numerical modelling OF PCFs

Lumerical Mode Solution (LMS) software was used to model the structure of the PCF. We choose the fused silica material in the system data as the substrate to design the PCFs. At the same time, the coefficients of the refractive index of silica according to Sellmeier equations (Eq. 1) [44] are also included in the data system for comparison and matching. The advantage is that lattice structure types are available in the system, so the circular lattice is marked because of its high symmetry. The air holes are designed in 8 layers evenly spaced and parallel along the core. Chloroform is filled into the hollow core of the PCF by declaring the Sellmeier coefficients according to according wavelength (λ) (Eq. 2) [36]. The perfectly matched layers that strongly absorb the waves coming from the calculated region without any reflection are the boundary conditions established for the LMS to be able to solve Maxwell's wave equations. The full-vector finite-difference eigenmode (FDE) method allows obtaining the field intensity profile of the fundamental mode of the PCFs with minimal loss. The propagation constant β with high accuracy is calculated using the "FDE

solver” thanks to the cross-section of the fiber being divided into small rectangular sections called “Yee’s mesh” [45]. This makes the optical properties in each of Yee’s meshes almost unchanged. An index averaging technique is used for the cells across interfaces at points lying on the surface between two media. The minimum mesh step of $10\text{--}6\ \mu\text{m}$ and 300 mesh cells without override regions is set for PCFs. The wavelength range investigated is $0.5\text{--}2.0\ \mu\text{m}$ which is compatible with existing LMS data.

$$n_{\text{SiO}_2}(\lambda) = \sqrt{1 + \frac{0.6961663\lambda^2}{\lambda^2 - 4.679148 \times 10^{-3}} + \frac{0.4079426\lambda^2}{\lambda^2 - 1.3512063 \times 10^{-2}} + \frac{0.8974794\lambda^2}{\lambda^2 - 97.93400254}} \quad (1)$$

$$n_{\text{CHCl}_3}(\lambda) = \sqrt{1 + \frac{1.04647\lambda^2}{\lambda^2 - 0.01048} + \frac{0.00345\lambda^2}{\lambda^2 - 0.15207}} \quad (2)$$

In our work, the optical properties of the PCFs are improved by a combination of three factors including the selection of the circular lattice, the chloroform filling in the hollow core of the PCF, and the lattice defects. Several previous publications [46, 47] verified that the difference in the air hole’s size of rings in the cladding strongly influences the nonlinear properties of PCFs. That means that every ring in the structure of PCFs has a profound effect on dispersion [48–50]. From this idea, we considered breaking the periodicity of the cladding rings to enhance the design freedom of the fiber to a large extent. So, we modeled PCFs with the air holes of the first ring near the core being smaller than others. Because the dispersion property is dominated by this ring including the shift of ZDW towards the long wavelength. But the remaining ring size is responsible for the loss in the fundamental mode or even the higher-order modes [46]. The filling factor d_1/Λ varies from 0.3 to 0.8 with each step of 0.5 (d_1 is the air hole’s diameter of the first ring), d_2/Λ is kept constant with a value of 0.95 (d_2 is the air hole’s diameter the second and other rings). We have carried out the simulations for different lattice constants ($\Lambda = 1.0\ \mu\text{m}$, $1.5\ \mu\text{m}$, $1.8\ \mu\text{m}$, and $2.0\ \mu\text{m}$). The radius of the hollow core is determined by the formula $R_c = (2\Lambda - 1.1d_1)/2$, which is also an important parameter to note in the design of PCF. Because the

core size must ensure good light confinement and match the actual manufacturing. The structural cross-section view of the circular chloroform-infiltrated PCFs is shown in Fig. 1a and b displays the light confined in the core for the structure $\Lambda = 2.0\ \mu\text{m}$; $d_1/\Lambda = 0.65$.

The real parts of the refractive index (n) of silica and chloroform depending on the investigated wavelength range is presented in Fig. 2a. The $\text{Re}[n_{\text{eff}}]$ values decrease with increasing wavelength. Although the real parts of the refrac-

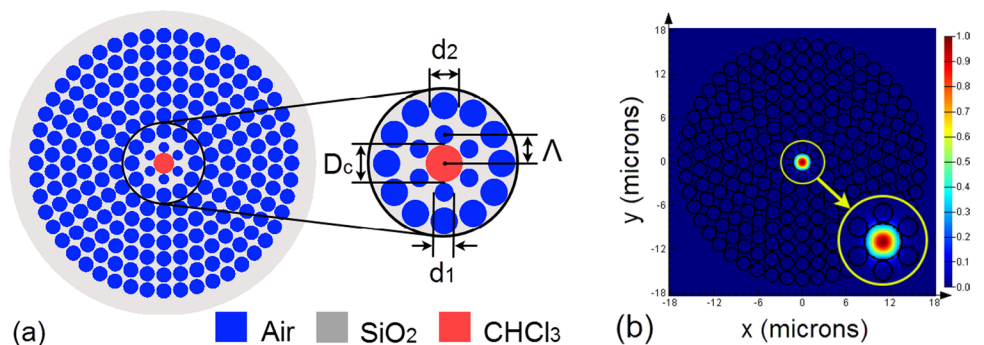
tive index of chloroform are lower than that of silica, the difference is not too large, and convenient for coupling with standard silica fibers. The transparency of chloroform is in the broad range of visible and near infrared wavelengths. The attenuation A depends on the adsorption wavelength λ calculated according to Eq. (3) [36]. Figure 2b shows a few adsorption peaks at $1.152\ \mu\text{m}$, $1.410\ \mu\text{m}$ and $1.691\ \mu\text{m}$, the strongest absorption peak at $1.691\ \mu\text{m}$ with k reaching the value of 2.65×10^{-4} , corresponding to A at this wavelength is equal to $85.6\ \text{dB}\cdot\text{cm}^{-1}$. Furthermore, chloroform has the lowest material dispersion in the visible region among common nonlinear liquids such as carbon disulfide and carbon tetrachloride. This implies that its applicability is suitable for new fields such as quality and security control or environmental monitoring as “some substances exhibit strong resonances related to rotational and vibrational resonances of various technologically vital molecules” [36, 51].

$$A = 10 \cdot \log [e^{A\pi k/\lambda}] \quad (3)$$

3 Simulation results and analysis

Chromatic dispersion is an important property of optical fiber in consideration for SC generations. The main nonlinear effects that appear to broaden the spectrum depend on

Fig. 1 Cross-section view of the circular chloroform-infiltrated PCFs **a**, the light confinement in the core of PCF with $\Lambda = 2.0\ \mu\text{m}$; $d_1/\Lambda = 0.65$ **b**



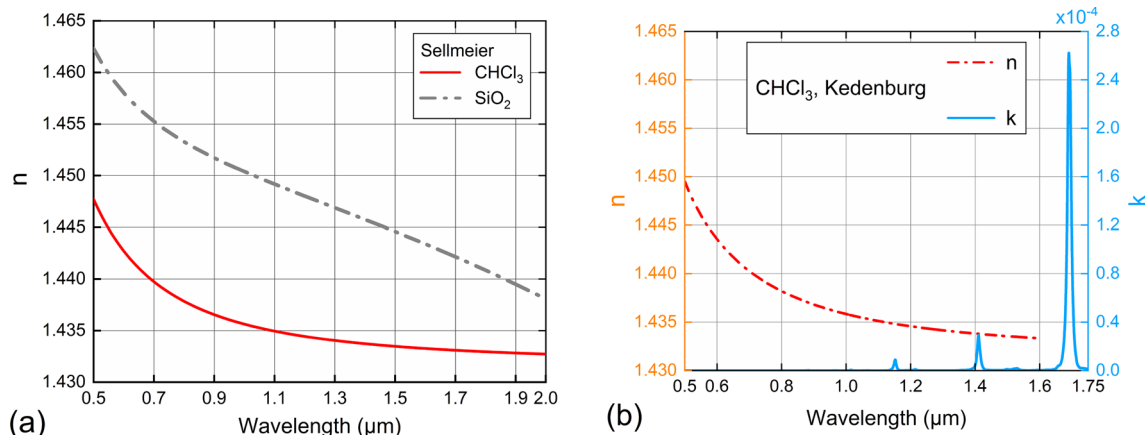


Fig. 2 The real parts of the refractive index n of chloroform and fused silica is extrapolated using Sellmeier’s equation **a** and the real n and imaginary k part of the refraction index of chloroform for the temperature of 20 °C is based on experimental data from [52] **b**

the dispersion properties of the PCF. It is the phenomenon where different pulse components propagate with different velocities, which is characterized by the propagation coefficient β . Background material types and defects in the lattice or geometry of the structure are responsible for altering the chromatic dispersion. Chromatic dispersion as a function of wavelength (λ), the speed of light in a vacuum (c), and the second derivative of the effective refractive index of the guided mode with respect to wavelength, is calculated by the formula (4) below [53]:

$$D = -\frac{\lambda}{c} \frac{\partial^2 \text{Re}[n_{\text{eff}}]}{\partial \lambda^2} \tag{4}$$

The second and higher dispersion are given by.

$$\beta = -\frac{\lambda^2 D(\lambda)}{2\pi c} \tag{5}$$

$$\beta_m = \left. \frac{d^m \beta}{d\omega^m} \right|_{\omega=\omega_0} \tag{6}$$

with ω_0 is the light center frequency.

Table 2 denotes that the higher-order dispersions have very small values and do not significantly influence the SC spectrum expansion (in the case of PCFs with $\Lambda = 1.0 \mu\text{m}$; $d_1/\Lambda = 0.65$ and $\Lambda = 2.0 \mu\text{m}$; $d_1/\Lambda = 0.3$). Therefore, we only analyze PCFs’ dispersion and nonlinear properties with the fundamental mode.

Figure 3 shows the simulated dispersion characteristics of the circular chloroform-infiltrated PCFs via a full-vector finite-difference eigenmode method. Both anomalous and all-normal chromatic dispersion are found in these PCFs. Owing to the large waveguide dispersion achieved with the small core diameter ($\Lambda = 1 \mu\text{m}$), the fibers considered in this work presented two ZDWs below 1.2 μm when the

Table 2 The coefficient of higher-order dispersion at the pump wavelength of the circular chloroform-infiltrated PCFs

Coefficients	$\Lambda = 1.0 \mu\text{m}; d_1/\Lambda = 0.65$	$\Lambda = 2.0 \mu\text{m}; d_1/\Lambda = 0.3$
β_2 (ps ² /m)	9.61×10^{-4}	-2.91×10^{-3}
β_3 (ps ³ /m)	-6.18×10^{-5}	1.11×10^{-4}
β_4 (ps ⁴ /m)	2.02×10^{-7}	-1.43×10^{-7}
β_5 (ps ⁵ /m)	4.27×10^{-10}	1.15×10^{-9}
β_6 (ps ⁶ /m)	2.32×10^{-11}	-1.06×10^{-11}
β_7 (ps ⁷ /m)	-4.91×10^{-13}	-4.01×10^{-15}
β_8 (ps ⁸ /m)	-5.45×10^{-15}	1.46×10^{-15}
β_9 (ps ⁹ /m)	1.68×10^{-16}	2.43×10^{-18}
β_{10} (ps ¹⁰ /m)	8.73×10^{-19}	-3.32×10^{-19}
β_{11} (ps ¹¹ /m)	-5.07×10^{-20}	-7.54×10^{-22}

d_1/Λ is greater than 0.65. It can be readily observed that reducing the filling factor d_1/Λ leads to lower chromatic dispersion profiles, and the saddles in the profiles become flatter and broader. In Fig. 3a, the dispersion of the fiber with $0.45 < d_1/\Lambda < 0.7$ is all-normal and the local maximum dispersion wavelengths are redshifted as the d_1/Λ decreases. As d_1/Λ continues to decrease, the dispersion curves are uplifted showing anomalous dispersion with one ZDW, the ZDWs perform a blue shift, this is not expected.

When Λ is larger ($\Lambda = 1.5 \mu\text{m}$) (Fig. 3b), the curves with ANDi characteristics are no longer observed, they are uplifted higher than the zero dispersion line and become anomalous dispersion curves with two ZDWs. More, local maximum dispersion wavelengths are also redshifted. For fibers with larger cores ($\Lambda = 1.8$ and $2.0 \mu\text{m}$) (Fig. 3c and d), the dispersion value increases with the increase of d_1/Λ in the wavelength region less than 1.7 μm . All dispersion curves intersect the zero dispersion line at a point corresponding to the anomalous dispersion profile with one

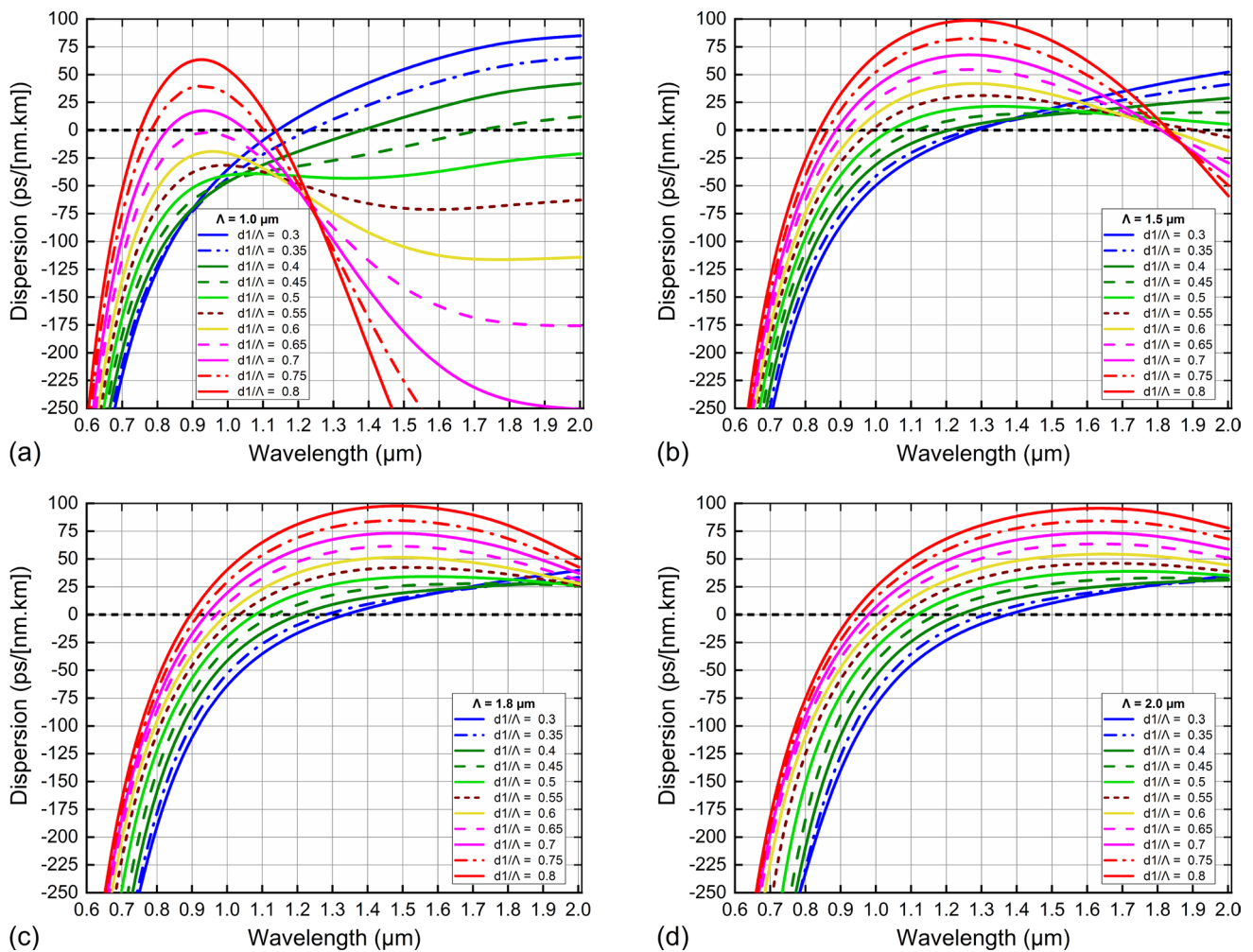


Fig. 3 The chromatic dispersion characteristics the circular chloroform-infiltrated PCFs with various values of d_1/Λ and $\Lambda = 1.0 \mu\text{m}$ **a**, $1.5 \mu\text{m}$ **b**, $1.8 \mu\text{m}$ **c**, and $2.0 \mu\text{m}$ **d**

ZDW. Furthermore the ZDWs are shifted towards shorter wavelengths as d_1/Λ increases. This suggests that structures with small d_1/Λ can be selected to obtain an appropriate ZDW. The structure with $\Lambda = 2.0 \mu\text{m}$, $d_1/\Lambda = 0.3$ has a flat dispersion curve and is closest to the zero dispersion line. In this case, material dispersion prevails. It can be seen that a reasonable adjustment of the air holes diameter of the rings in the cladding is an advantage factor for dispersion control.

The choice of pump wavelength in SC generation depends on the shift of the zero dispersion wavelength. This is an important factor affecting the SC spectrum expansion, moreover, the proposed pump wavelengths must satisfy conditions such as the dispersion value being small enough to improve SC performance and matching commercial lasers. Most of the ZDWs1 of PCFs with large Λ decrease with

increasing the filling factor, except PCFs with $\Lambda = 1 \mu\text{m}$ (Table 3).

The fundamental mode dispersion parameters play a very important role in SC generation, because they would determine which PCF produces the broad spectrum. The fiber materials and structures often affect various aspects of dispersion such as value, the number of ZDWs, flatness. PCFs with many ZDWs have a small range of variation that can make the dispersion profile flat [54]. In addition, coherent SC in guided structures can be generated by flat-dispersion PCFs with lower values [55]. Also, the combination of different nonlinear properties of an optical medium can govern the influence of the main effects occurring during SC generation including soliton dynamics and non-solitonic dispersive wave (DW). The above analysis leads to the recommendation of selecting two fibers with optimal dispersion for SC generation. The

Table 3 ZDWs of the circular chloroform-infiltrated PCFs

d_1/Λ	$\Lambda = 1.0$ (μm)		$\Lambda = 1.5$ (μm)		$\Lambda = 1.8$ (μm)		$\Lambda = 2.0$ (μm)	
	ZDWs1	ZDWs2	ZDWs1	ZDWs2	ZDWs1	ZDWs2	ZDWs1	ZDWs2
0.3	1.141		1.286		1.335		1.374	
0.35	1.23		1.268		1.28		1.308	
0.4	1.381		1.207		1.205		1.234	
0.45	1.716		1.113		1.135		1.17	
0.5			1.12		1.079		1.116	
0.55			0.986	1.904	1.033		1.071	
0.6			0.947	1.83	0.998		1.034	
0.65			0.914	1.818	0.968		1.004	
0.7	0.827	1.053	0.886	1.815	0.941		0.978	
0.75	0.781	1.103	0.862	1.827	0.918		0.954	
0.8	0.75	1.136	0.839	1.837	0.895		0.931	

first fiber, #F₁ ($\Lambda = 1.0 \mu\text{m}$ and $d_1/\Lambda = 0.65$), has an ANDi with the local maximum dispersion wavelengths closest to the zero dispersion. With a small dispersion value of -1.629 ps/nm.km at a pump wavelength of $0.945 \mu\text{m}$ (Fig. 4a), this fiber is expected to produce a broad SC spectrum and high coherence due to the SPM effect. Meanwhile, the soliton dynamics will dominate the SC spectral expansion when the #F₂ fiber ($\Lambda = 2.0 \mu\text{m}$ and $d_1/\Lambda = 0.3$) is pumped in an anomalous dispersion region at the pump wavelength of $1.4 \mu\text{m}$. The #F₂ fiber has the flattest dispersion among dispersion curves with $\Lambda = 2.0 \mu\text{m}$. It has a low dispersion value of 2.619 ps/(nm.km) at the pump wavelength (Fig. 4a). Several previous publications on hexagonal chloroform-infiltrated PCFs showed rather high dispersion values at the pump wavelength. At $1.06 \mu\text{m}$ pumping wavelength, the optimal fiber with ANDi in [35] has about 12 to 30 times more dispersion than in this work. The dispersion value of about 14 times for ANDi and 3 times for anomalous dispersion, at $0.92 \mu\text{m}$ pump wavelength and $1.03 \mu\text{m}$, respectively, were reported for two fibers proposed for SC generation in [36].

The generation of broad-spectrum SC is also affected by the nonlinear properties of the optical medium because they contribute to the generation of new frequencies through nonlinear phenomena such as FWM, SPM, SF, SSFS, etc. ... The nonlinear coefficient quantifies the strength of a nonlinear interaction, which often strongly influences the peak power of the input pulse, is determined by the following formula (7) [4]:

$$\gamma(\lambda) = 2\pi \frac{n_2}{\lambda A_{\text{eff}}} \tag{7}$$

where A_{eff} is the area of the effective mode for the basic mode of the fiber and n_2 is the nonlinear refractive index of the optical material. The effective mode area for the

fundamental mode is a quantitative measure of the area which a waveguide or fiber mode effectively covers in the transverse dimensions, can be calculated by using formula (8) [56]:

$$A_{\text{eff}} = \frac{\left(\int_{-\infty}^{\infty} \int_{-\infty}^{\infty} |E|^2 dx dy \right)}{\int_{-\infty}^{\infty} \int_{-\infty}^{\infty} |E|^4 dx dy} \tag{8}$$

where E is the transverse electric field over the cross-section of the PCF.

“Confinement loss is the loss which should be minimized so that the light modes to be transmitted is confined in the core and it should not be dispersed” [57], can be computed on basis of imaginary part of effective refractive index and wavelength:

$$L_c = 8.686 \frac{2\pi}{\lambda} \text{Im}[n_{\text{eff}}(\lambda)] \tag{9}$$

Figure 4b, c, and d display the dependence between the nonlinear coefficient, effective mode area, and confinement loss of the fundamental mode on the wavelength for #F₁ and #F₂ fibers. The nonlinear coefficient of fiber #F₁ is higher than #F₂ for all wavelengths. The γ of the two proposed fibers is relatively high at the pump wavelength of $763.313 \text{ W}^{-1}.\text{km}^{-1}$ and $63.913 \text{ W}^{-1}.\text{km}^{-1}$, respectively. Since the effective mode area is inversely proportional to the nonlinear coefficient, fiber #F₂ has a larger A_{eff} . The A_{eff} of #F₂ is $11.524 \mu\text{m}^2$, about 8 times the value of #F₁ ($1.43 \mu\text{m}^2$) at the respective pump wavelengths. Fibers with large core sizes often exhibit worse core light confinement, so #F₂ fibers have a higher confinement loss. This involves leakage of modes from the core

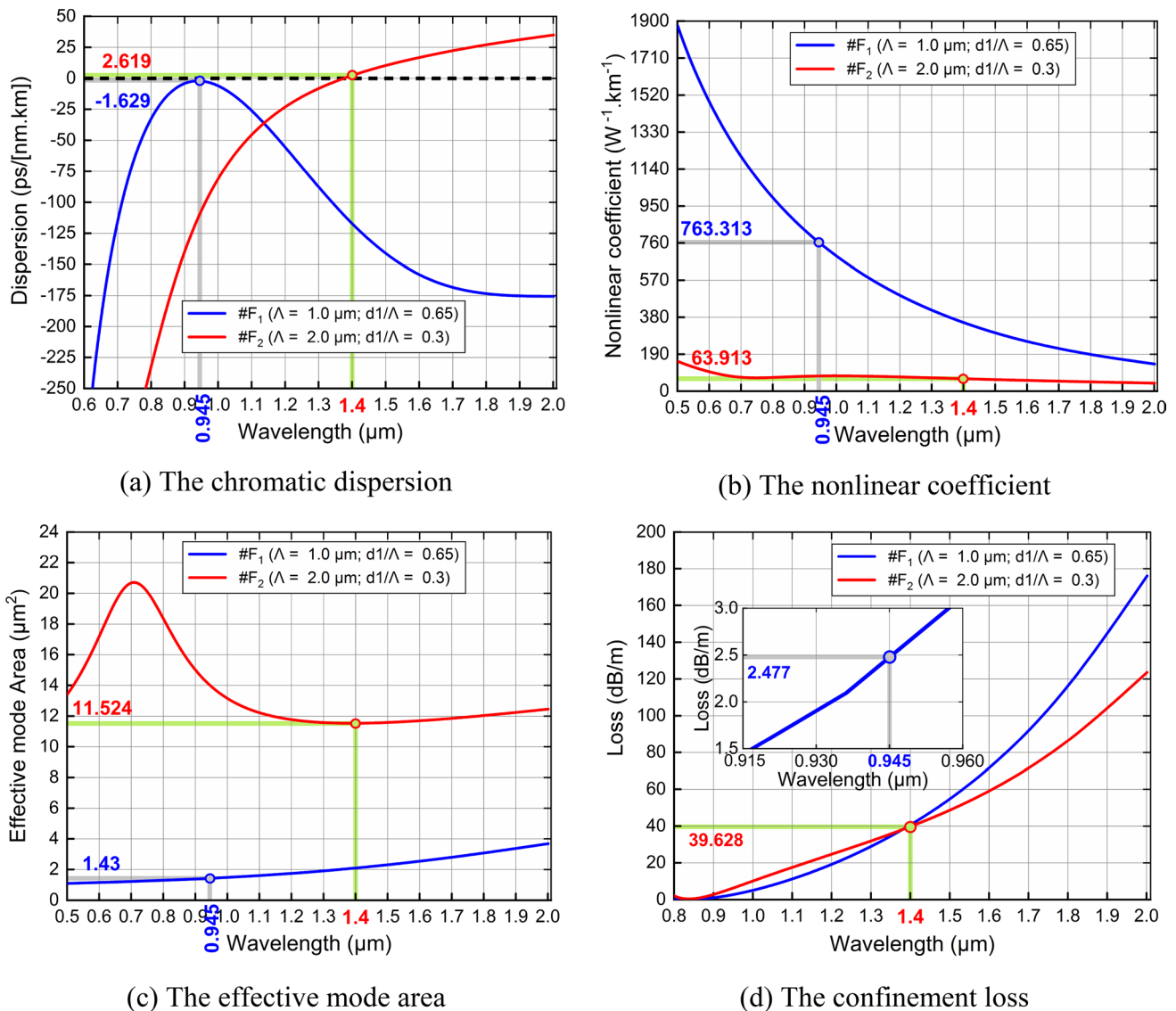


Fig. 4 The optical characteristics of the fundamental mode for #F₁ and #F₂ fibers

to the cladding or between air holes in the cladding. So, the core size limitation is also necessary in the design and numerical simulation of PCFs. If the core size is too large, of course, it will negatively affect the fiber loss, but if the core size is too small, it will be difficult to fabricate the fiber in practice. The L_c value of #F₂ 39.628 dB/m is about 16 times that of fiber #F₁ (2.477 dB/m). We expect that a larger L_c value of #F₂ will have a small effect on the SC spectral broadening (we will discuss in the next section) because #F₂ has a rather small anomalous dispersion at the pump wavelength. Table 4 manifests the structural parameters and the characteristic quantities of the two proposed fibers at the pump wavelength in comparison with some other liquid-infiltrated PCFs. It is essential for broad

spectrum SC that mostly the fundamental mode is pumped due to the lowest effective mode area leading to the highest nonlinearity. So, these structures offer low dispersion and suitable nonlinearity for optimum SC in PCF.

4 Supercontinuum generation in proposed fiber

The higher-order dispersions are simulated to the 11th order and presents a rather small value, verified in the Table 2. The impact of the dispersive and nonlinear processes on pulses shapes and SC spectra when the ultrashort optical pulses propagate inside the optimal PCFs are numerically studied

Table 4 The structure parameters and the characteristic quantities of #F₁ and #F₂ fibers at the pump wavelength in comparison with some other liquid-infiltrated PCFs

#	R _c (μm)	Λ (μm)	d ₁ /Λ	Pump wave-length (μm)	A _{eff} (μm ²)	γ (W ⁻¹ .km ⁻¹)	D (ps/nm.km)	L _c (dB/m)
#F ₁	0.643	1.0	0.65	0.945	1.43	763.313	-1.629	2.477
#F ₂	1.67	2.0	0.3	1.40	11.524	63.913	2.619	39.628
#F ₁ [36] chloroform	0.643	1.0	0.65	1.03	1.5	1290	-24	-
#F ₂ [36] chloroform	1.643	2.0	0.65	1.03	4.48	440	7.6	-
#I_0.3 [19] toluene	3.28	2.0	0.3	1.55	7.79	2132.575	-7.784	40
#I_0.35 [19] toluene	2.8	2.0	0.5	1.55	78.9	2890.276	-1.19	120
#F ₁ [18] tetrachloroethylene	1.28	1.5	0.4	1.56	433.2	156.9	-15.0	4.0
#F ₂ [18] tetrachloroethylene	3.753	4.0	0.45	1.56	16.67	40.79	3.20	4.2
#F ₃ [18] tetrachloroethylene	1.198	1.5	0.55	1.03	359.1	189.3	-4.85	5.3
#F ₁ [13] carbon tetrachloride	1.125	1.5	0.45	1.35	11.83	-	12.0	1.85
#F ₂ [13] carbon tetrachloride	3.56	4.0	0.8	1.064	10.58	-	-4.37	1.58

using the generalized nonlinear Schrödinger equation which is in the form of [1]:

$$\begin{aligned} \partial_z \tilde{A} - i\tilde{\beta}(\omega)\tilde{A} - \frac{\tilde{\alpha}(\omega)}{2}\tilde{A} \\ = i\gamma \left(1 + \frac{\omega - \omega_0}{\omega_0} \right) \tilde{A} F \left[\int_{-\infty}^{\infty} R(T') |A|^2 (T - T') dT' \right] \end{aligned} \quad (10)$$

where $A(z, \omega)$ is Fourier transform of the amplitude of a pulse $A(z, T)$, and $R(T')$ is the Raman response function. The left side of Eq. 10 depicts the linear propagation effects of the fiber, $\tilde{\alpha}$ and $\tilde{\beta}$ are attenuation and dispersion in the frequency domain, respectively. The right-hand side of the Eq. 10 describes the nonlinear effects which depend on the nonlinear optical response of chloroform determined by the combination of the bound-electronic and nuclear contribution. Nonlinear parameters used in simulations [58]. The subscripts el, d, l, c indicate the following mechanisms: the bound-electronic, molecular reorientation, molecular interaction and collision induced, respectively. Where $n_{2,el} = 0.41 \times 10^{-19} \text{ m}^2 \text{ W}^{-1}$, $n_{2,d} = 0.75 \times 10^{-19} \text{ m}^2 \text{ W}^{-1}$, $\tau_{r,d} = 0.25 \text{ ps}$, $\tau_{f,d} = 0.18 \text{ ps}$, $n_{2,l} = 0.4 \times 10^{-19} \text{ m}^2 \text{ W}^{-1}$, $n_{2,c} = 0.08 \times 10^{-19} \text{ m}^2 \text{ W}^{-1}$, $\tau_{r,c} = 0.1 \text{ ps}$, $\tau_{f,c} = 0.1 \text{ ps}$.

Both all-normal and anomalous dispersion of #F₁ and #F₂ fibers clearly show the dominance of different nonlinear effects on the characteristics of the SC spectrum. #F₁ fiber provides a broad, low-noise SC spectrum while #F₂ fiber generates a much broader SC spectrum despite more noise. The large difference between the nonlinear refractive index of chloroform and silica, the low dispersion, and the small

effective mode area are necessary for us to simulate SC generation with low peak power.

In the first step of this section, we analyze the simulation results of a laser pulse propagating in a 10 cm long #F₁ optical fiber excited at a wavelength of 0.945 μm. The width of the input pulse is set as 90 fs. The influence of the input pulse energy (E) on the broadband spectra is shown in Fig. 5a. The spectra is broadened obviously when the E increases from 0.01 to 0.1 nJ corresponding to the peak power (P) rising from 0.11 kW to 1.1 kW. However, the spectral width changes slightly when the E increases to 0.13 nJ ($P = 1.44 \text{ kW}$). Thus, $P = 1.44 \text{ kW}$ is considered as the limiting peak power to broaden the spectra. The fairly flat profile with small fluctuations (spectral levels below 10 dB in this work) of the output pulse is typical of pumped fibers in the ANDi regime. Also, the spectral fluctuations on the longer wavelength side are significantly reduced as the peak power increases. The nonlinear optical process, namely SPM and OWB, contribute to the pulses' spectral broadening in the #F₁ fiber with the ANDi regime. With an input peak power as small as 0.11 kW (corresponding to an input pulse energy of 0.01 nJ), the spectrum is expanded symmetrically only by the SPM. As the input pulse energy increases further, SPM is the dominant expansion mechanism in the initial stage. Then, new frequencies are created by overlapping of different pulse spectral components due to the OWB associated with FWM. That leads to a significant blue shift and red shift of the spectrum. However, the spectrum broadening on the short wavelength side is less efficient than that on the long wavelength side causing the spectral shape to be asymmetrical. The steeper dispersion profile at short

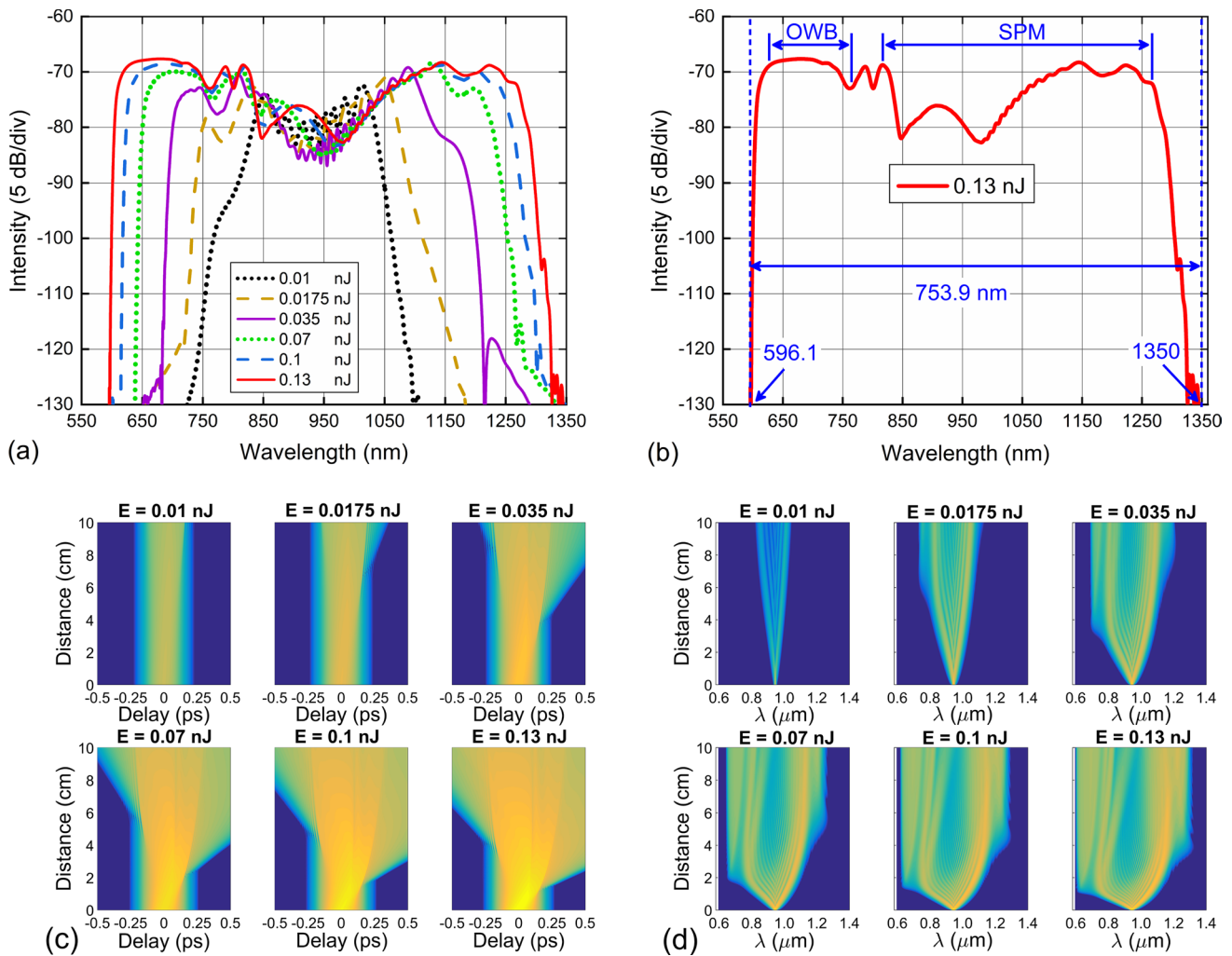


Fig. 5 For #F₁ fiber (length of 10 cm): **a** the output spectrum for various input pulse energies when using pump pulses with 0.945 μm pump wavelength and 90 fs duration, **b** the output spectrum with the

input pulse energy of 0.13 nJ, **c** the temporal profile at various propagation length, and **d** the pulse evolution of the SC along with fiber

wavelengths is responsible for this phenomenon, although the higher input energy can be used to increase intensity at the trailing edge [59, 60]. When the E is increased to 0.13 nJ ($P = 1.44$ kW), the long wavelength edge of SC spectrum was broadened, and the widest SC covering from 596.1 to 1350 nm was generated, as depicted in Fig. 5b. In fact, it is the absorption of chloroform at long wavelengths and the increase in the effective mode area of #F₁ fiber at long wavelengths that reduces the spectral expansion even though P is further increased. One of the ways to increase the bandwidth further is to reduce the effective mode area, i.e., increase the nonlinear coefficient of the fiber by reducing the core diameter. However, we should consider the coupling efficiency in fiber fabrication. It will be lost if the core size is further decreased and therefore decrease input pulse energy when coupled with standard single-mode fiber in an all-fiber

system [6]. Hence, $P = 1.44$ kW is the maximum peak power used in this #F₁ fiber.

Figure 5c and d testify the temporal profile at various propagation lengths, and the pulse evolution of the SC along with fiber. At the beginning of propagation, the interaction between the SPM and the normal dispersion leads to a symmetrical spectral broadening during the first few millimeters. OWB occurs first at 8 cm of propagation towards the short wavelengths side with $E = 0.175$ nJ. For $E = 0.035$ nJ, the OWB occurs at a distance of 4 cm and 8 cm of propagation on the short and long wavelength sides, respectively. As the input pulse energy increases further, the OWB appears at shorter propagation distances. When E reaches a peak value of 0.13 nJ (1.44 kW of the peak power), and the symmetrical expansion in the first few millimeters of propagation is attributed to the SPM. When the excitation pulse propagates at a distance of 1 cm, the OWB appears early

on the blueshift side, creating a new wavelength band and broadening the short wavelength components to 596.1 nm. During further propagation, the high slope of the dispersion profile on the short wavelength side is responsible for the inhibition of spectral expansion. On the redshift side, a new wavelength band is generated at 4 cm of propagation and extends the long wavelengths up to 1350 nm due to the appearance of OWB. At this point, the spectrum can expand further. However, the limitation here is related to the optical fiber's nonlinear reduction due to the increase of effective mode area at long wavelength. The contiguous spectral components overlapping each other in a too short period cannot effectively contribute to further spectral widening, which is the cause of the group delay of the pulse being stretched out in the time domain (Fig. 5c).

In the second step of this section, we have carried out nonlinear optical characterizations by pumping the #F₂ fiber

at 1.4 μm in an anomalous dispersion regime. A pulse of width 45 fs is propagated in 12 cm of fiber length. The effect of the input pulse energy on the bandwidth of the generated spectrum is observed in Fig. 6a. It illustrates that the broadening of the output spectra increases with a further increase in input pulse energy. With a minimum input pulse energy of 0.01 nJ (corresponding to 0.22 kW peak power), the SPM causes the spectrum to broaden symmetrically. Soliton starts to occur, causing the pulse to lose symmetry with $E=0.075$ ($P=1.67$ kW). As E increases further, the pulse spectrum becomes broader but noisier and the spectral width is much larger than that of the pumped #F₁ fiber in the ADNi regime. This spectrum characterization indicates that the typical SC growth is connected to the dynamics of soliton propagation and break-up in the anomalous dispersion regime [1]. Namely, in the initial stage of only a few millimeters of propagation, the SPM followed by pulse

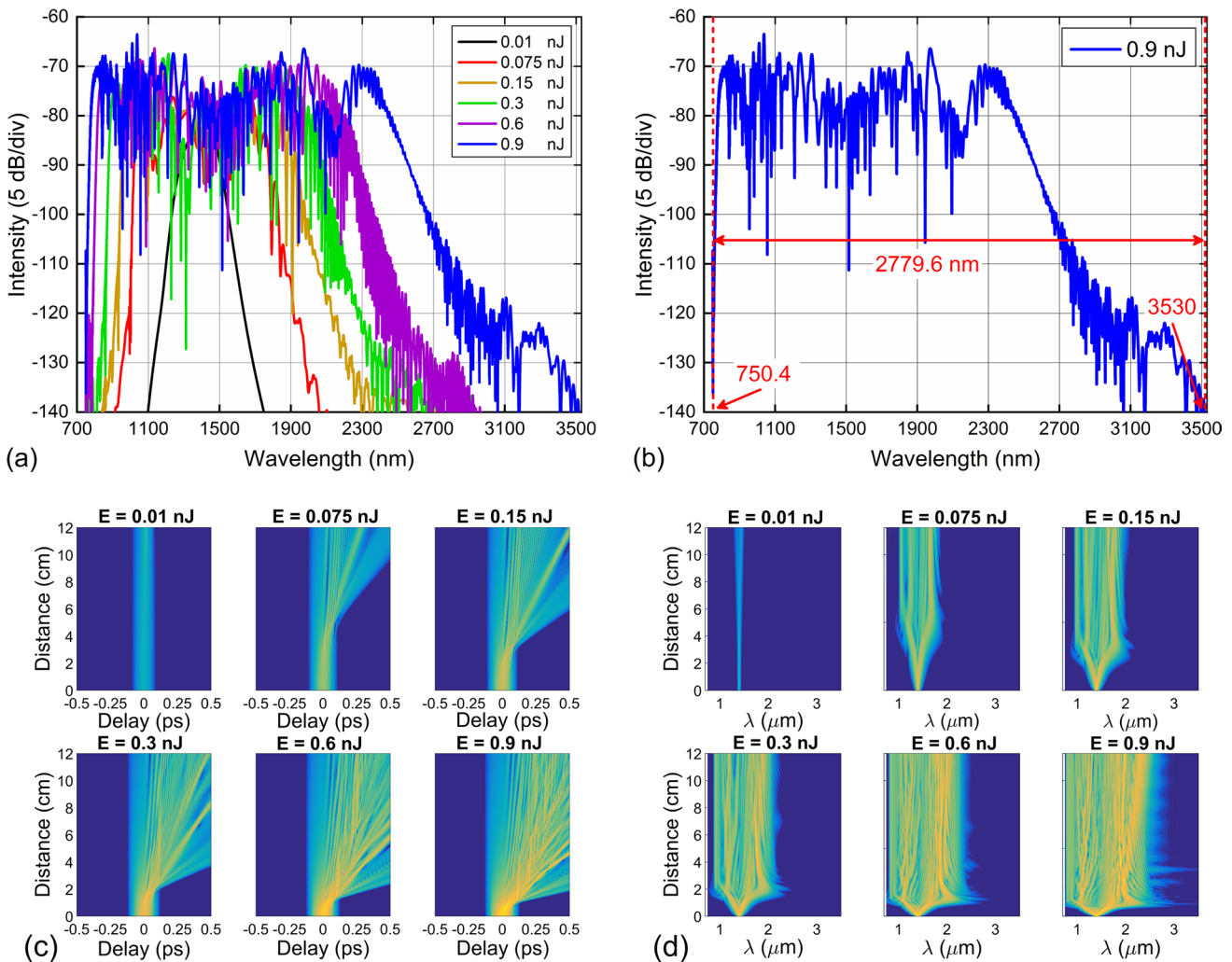


Fig. 6 For #F₂ fiber (length of 12 cm): **a** the output spectrum for various input pulse energies when using pump pulses with 1.4 μm pump wavelength and 45 fs duration, **b** the output spectrum with the input

pulse energy of 0.9 nJ, **c** the temporal profile at various propagation length, and **d** the pulse evolution of the SC along the fiber

break-up affects the input pulse extension. Next, the SSFS, due to intrapulse Raman scattering, strongly dominates the spectral broadening for longer wavelengths. In addition, the #F₂ fiber is pumped at a wavelength of 1.4 μm close to its ZDW (1.374 μm), so the solitons generated in the anomalous dispersion regime have shed energy into dispersive waves (DW) in the normal dispersion regime [1]. The influence of nonlinear effects on spectral expansion includes SSFS (red-shift side) and DW generation (blue-shift side). Therefore, the bandwidth gets larger for higher peak power. Our numerical simulation shows that the generated SC for the highest peak power of 20 kW ($E=0.9$ nJ) reached 2779.6 nm (Fig. 6b).

Figure 6c and d display the temporal profile at various propagation lengths, and the pulse evolution of the SC along the fiber #F₂. When the input pulse energy reaches 0.9 nJ (corresponding to 20 kW peak power), there is a preliminary symmetric pulse broadening as a result of the influence of the SPM at about the first 5 mm of the propagation length. Then, further propagation is aided by soliton fission at about 1 cm of fiber length with the involvement of Raman scattering events. The presence of higher-order dispersion increases the SF process, so a series of fundamental solitons, which are both spectrally more extensive and temporally narrower, are created from a higher-order soliton [61]. The first fundamental soliton having the shortest duration and broad spectrum with the highest energy undergoes SSFS shift towards the red-side due to stimulated Raman scattering. As a result, there is a continual redshift of the long-wavelength elements, spectrum drifts right side to 3500 nm. At the same time, the first ejected soliton has a reduced speed due to the high dispersion slope being caught up by the DW and new wavelength components are generated through the FWM effect resulting in a slight blue shift in the spectrum. The spectrum is extended to a wavelength of 750.4 nm, which is less than the pump wavelength. The pulse peak power is also important to improve the bandwidth of the SC, this is also expected by increasing the peak power even further. However, the limitation of spectral expansion is attributed to fiber loss due to the high absorption of chloroform in the long wavelength region and the low nonlinear coefficient of 63.913 W⁻¹.km⁻¹ of the #F₂ fiber. It can be seen that a value of 20 kW is the limit for the expectation of further increase in peak power. So, a broadband supercontinuum generation with a spectral width of about 2779.6 nm obtained after a pulse propagation of only 1 cm benefits from the flat and low anomalous dispersion of the #F₂ fiber.

5 Conclusion

The circular chloroform-infiltrated PCFs with reasonable modification of structural parameters have been stated in this study showing high dispersion control for efficient SC generation. By selecting suitable sets of fiber parameters, we propose two optimal PCFs to investigate SC generation processes. Broad SC spectra have been obtained and found in good agreement with numerical predictions, thus confirming the simulated dispersion properties. The main results obtained are as follows:

For #F₁ fiber ($\Lambda=1.0$ μm and $d_1/\Lambda=0.65$): The dispersion as small as -1.629 ps/nm.km at 0.945 μm pump wavelength is found with ADNi regime. The rather high nonlinear coefficient of 763.313 W⁻¹.km⁻¹ is also a necessary factor contributing to the SC spectrum expansion with a small peak power of 1.44 kW. SPM followed by OWB are the main nonlinear effects that cause the spectrum to broaden with a width of 753.9 nm when the excitation pulse propagates within 10 cm of the fiber length. In the work [36], chloroform-infiltrated PCF with the ANDi regime emitted a wide SC spectrum of 660 nm with a peak power 1.7 times higher than this study despite the short fiber length of only 1 cm. Compared with other nonlinear fluids-infiltrated PCFs, #F₁ fiber achieves a broader spectrum with 1.8 times [13] and 5 times lower peak power [19], respectively. With benzene-filled PCF, the work [25] demonstrated an SC spectrum twice as broad as this work but about 38 times higher peak power. Similarly, nitrobenzene and tetrachlorethylene-infiltrated PCF permeable also give about twice as wide spectrum but about 3.9 times and 12 times more peak power, respectively (Table 1).

For #F₂ fiber ($\Lambda=2.0$ μm and $d_1/\Lambda=0.3$): This fiber has flat and low anomalous dispersion, the dispersion value at 1.4 μm pump wavelength is 2.619 ps/nm.km. Despite having a relatively low nonlinear coefficient of 63.913 W⁻¹.km⁻¹ and a rather high confinement loss of 39.628 dB/m, this fiber generates a broad SC spectrum of 2779.6 nm with the main dominance of the soliton dynamics. An input pulse with a peak power of 20 kW propagates in 12 cm of the fiber length. Table 1 also shows that compared with some other previous publications on chloroform-filled PCF, we achieved a spectrum of about 2.7 times broader with 2.35 times lower peak power [35]. Although #F₂ has the advantage of 2 to 3 times wider spectrum, the peak power is nearly 10 times higher than the reports [34, 36]. When using other nonlinear liquids to fill PCFs, such as tetrachlorethylene, the work [18] showed that the SC spectrum is 1.6 to 2.7 times narrower than this study in spite of similar peak powers. The work [25] showed that with higher peak power, the PCF filled by benzene emits SC with a narrower spectrum. However, for toluene-infiltrated PCFs, the publication [20] indicates that a broad SC spectrum above 2000 nm can be achieved

with only 0.56 kW peak power when PCF was pumped at 1.55 μm .

These results anyway confirm the great potential of $\#F_1$ and $\#F_2$ fibers for the efficient supercontinuum generation. In addition, in our study, SC spectrum with broadband is generated even though the input pulse peak power is small, benefiting from the high non-linearity of chloroform. These fibers can be a new class of optical fibers that effectively replace traditional glass-core fibers and such broad SC bandwidth could be advantageous for wide applications in the fields of spectroscopy, biomedical, and sensing. However, before they can become really useful in applications, the problems associated with the fusion splicing of liquid core PCFs and standard silica fibers need to be considered. This is still of interest to research groups, although various modifications of the fusion splicing methods have been proposed to date.

Author contributions All authors contributed to the study conception and design. Material preparation [LCV], data collection [LCV] and analysis were performed by [TNT]. The first draft of the manuscript was written by [TNT] and all authors commented on previous versions of the manuscript. All authors read and approved the final manuscript.

Funding This research is funded by University of Education, Hue University under grant number NCM. T.23–02.

Data availability statement No data availability statement.

Declarations

Conflict of interest The authors declare that they have no conflict of interest.

References

- Dudley, J.M., Taylor, J.R.: Supercontinuum generation in optical fibers. Camb. Univ. Press (2010). <https://doi.org/10.1017/CBO9780511750465>
- Van, L.C., Tran, B.T.L., Thi, T.N., Trong, D.H., Van, T.D., Mai, T.D., Ngoc, H.T., Doan, T.T., Quoc, K.D.: Comparison of supercontinuum generation spectral intensity in benzene-core PCFs with different types of lattices in the claddings. *Opt. Quant. Electron.* **54**, 840 (2022). <https://doi.org/10.1007/s11082-022-04218-1>
- Lanh, C.V., Bao, T.L.T., Trong, D.V., Ngoc, V.T., Thuy, N.T., Hong, P.N.T., Minh, H.T.N., Van, T.H.: Supercontinuum generation in highly birefringent fiber infiltrated with carbon disulfide. *Opt. Fiber Technol.* **75**, 103151 (2023). <https://doi.org/10.1016/j.yofte.2022.103151>
- Lanh, C.V., Hieu, V.L., Nguyen, D.N., Ngoc, V.T.M., Quang, H.D., Van, T.H., Thuy, N.T., Bien, C.V.: Modelling of lead-bismuth gallate glass ultra-flatted normal dispersion photonic crystal fiber infiltrated with tetrachloroethylene for high coherence mid-infrared supercontinuum generation. *Laser Phys.* **32**, 055102–055112 (2022). <https://doi.org/10.1088/1555-6611/ac599b>
- Hoang, V.T., Kasztelanic, R., Anuszkiewicz, A., Stepniewski, G., Filipkowski, A., Ertman, S., Pysz, D., Wolinski, T., Xuan, K.D., Klimczak, M., Buczynski, R.: All-normal dispersion supercontinuum generation in photonic crystal fibers with large hollow cores infiltrated with toluene. *Opt. Mater. Express* **8**(11), 3568–3582 (2018). <https://doi.org/10.1364/OME.8.003568>
- Hoang, V.T., Kasztelanic, R., Filipkowski, A., Stepniewski, G., Pysz, D., Klimczak, M., Ertman, S., Long, V.C., Woliński, T.R., Trippenbach, M., Xuan, K.D., Śmietana, M., Buczyński, R.: Supercontinuum generation in an all-normal dispersion large core photonic crystal fiber infiltrated with carbon tetrachloride. *Opt. Mater. Express* **9**(5), 2264–2278 (2019). <https://doi.org/10.1364/OME.9.002264>
- Thuy, N.T., Duc, H.T., Bao, T.L.T., Lanh, C.V.: Flat-top and broadband supercontinuum generation in CCl_4 -filled circular photonic crystal fiber. *J Nonlin. Opt. Phys. Mater.* (2022). <https://doi.org/10.1142/S021886352350042X>
- Sanders, S.T.: Wavelength-agile fiber laser using group-velocity dispersion of pulsed super-continua and application to broadband absorption spectroscopy. *Appl. Phys. B* **75**, 799–802 (2002). <https://doi.org/10.1007/s00340-002-1044-z>
- Sanchita, S., Al-Tabatabai, K.F., Amrindra, P., Dhasarathan, V., AsifArefin, M., MdKabirul, I.: D-shape photonic crystal fiber for optical coherence tomography: design and analysis. *Opt. Eng.* **60**(12), 127109 (2021). <https://doi.org/10.1117/1.OE.60.12.127109>
- Chetan, P., Clemens, F.K.: Supercontinuum radiation in fluorescence microscopy and biomedical imaging applications. *J. Opt. Soc. Am. B* **36**(2), A139–A153 (2019). <https://doi.org/10.1364/JOSAB.36.00A139>
- Jahromi, K.E., Pan, Q., Høgstvedt, L., Friis, S.M., Khodabakhsh, A., Moselund, P.M., Harren, F.J.: Mid-infrared supercontinuum-based upconversion detection for trace gas sensing. *Opt. Express* **27**(17), 24469–24480 (2019). <https://doi.org/10.1364/OE.27.024469>
- Nishizawa, N., Kawagoe, H., Yamanaka, M., Matsushima, M., Mori, K., Kawabe, T.: Wavelength dependence of ultrahigh-resolution optical coherence tomography using supercontinuum for biomedical imaging. *IEEE J. Sel. Topics Quant. Electron.* **25**(1), 1–15 (2018). <https://doi.org/10.1109/JSTQE.2018.2854595>
- Dinh, Q.H., Pniewski, J., Van, H.L., Ramaniuk, A., Long, V.C., Borzycki, K., Xuan, K.D., Klimczak, M., Buczyński, R.: Optimization of optical properties of photonic crystal fibers infiltrated with carbon tetrachloride for supercontinuum generation with subnanosecond femtosecond pulses. *Appl. Opt.* **57**(14), 3738 (2018). <https://doi.org/10.1364/AO.57.003738>
- Guo, Y., Yuan, J., Wang, K., Wang, H., Cheng, Y., Zhou, X., Yan, B., Sang, X., Yu, C.: Generation of supercontinuum and frequency comb in a nitrobenzene-core photonic crystal fiber with all-normal dispersion profile. *Opt. Commun.* **481**(15), 126555 (2021). <https://doi.org/10.1016/j.optcom.2020.126555>
- Van, L.C., Thi, T.N., Trong, D.H., Tran, B.T.L., Minh, N.V.T., Van, T.D., Canh, T.L., Dinh, Q.H., Quoc, K.D.: Comparison of supercontinuum spectrum generating by hollow core PCFs filled with nitrobenzene with different lattice types. *Opt. Quant. Electron.* **54**, 300 (2022). <https://doi.org/10.1007/s11082-022-03667-y>
- Lanh, C.V., Van, T.H., Van, C.L., Borzycki, K., Khoa, D.X., Vu, T.Q., Trippenbach, M., Buczyński, R., Pniewski, J.: Supercontinuum generation in photonic crystal fibers infiltrated with nitrobenzene. *Laser Phys.* **30**(3), 035105 (2020). <https://doi.org/10.1088/1555-6611/ab6f09>
- Hieu, V.L., Van, T.H., Stepniewski, G., Trung, L.C., Ngoc, V.T.M., Kasztelanic, R., Klimczak, M., Pniewski, J., Khoa, X.D., Heidt, A.M., Buczyński, R.: Low pump power coherent supercontinuum generation in heavy metal oxide solid-core photonic crystal fibers infiltrated with carbon tetrachloride covering 930–2500 nm. *Opt. Express* **29**(24), 39586–39600 (2021). <https://doi.org/10.1364/OE.443666>

18. Hieu, V.L., Van, T.H., Hue, T.N., Van, C.L., Buczynski, R., Kasztelan, R.: Supercontinuum generation in photonic crystal fibers infiltrated with tetrachloroethylene. *Opt. Quant. Electron.* **53**, 187 (2021). <https://doi.org/10.1007/s11082-021-02820-3>
19. Lanh, C.V., Anuszkiewicz, A., Ramaniuk, A., Kasztelan, R., Khoa, X.D., Trippenbach, M., Buczynski, R.: Supercontinuum generation in photonic crystal fibres with core filled with toluene. *J. Opt.* **19**, 125604 (2017). <https://doi.org/10.1088/2040-8986/aa96bc>
20. Thuy, N.T., Duc, H.T., Bao, T.L.T., Trong, D.V., Lanh, C.V.: Optimization of optical properties of toluene-core photonic crystal fibers with circle lattice for supercontinuum generation. *J. Opt.* (2022). <https://doi.org/10.1007/s12596-021-00802-y>
21. Thuy, N.T., Duc, H.T., Lanh, C.V.: Supercontinuum generation in ultra-flattened near-zero dispersion PCF with C7H8 infiltration. *Opt. Quant. Electron.* **55**, 93 (2023). <https://doi.org/10.1007/s11082-022-04351-x>
22. Ahmad, R., Komanec, M., Zvanovec, S.: Ultra-wideband mid-infrared supercontinuum generation in liquid-filled circular photonic crystal fiber. *J. Nanophoton.* **14**(2), 026016 (2020). <https://doi.org/10.1117/1.JNP.14.026016>
23. Junaid, S., Bierlich, J., Hartung, A., Meyer, T., Chemnitz, M., Schmidt, M.A.: Supercontinuum generation in a carbon disulfide core microstructured optical fiber. *Opt. Express* **29**(13), 19891–19902 (2021). <https://doi.org/10.1364/OE.2426313>
24. Churin, D., Nguyen, T.N., Kieu, K., Norwood, R.A., Peyghambarian, N.: Mid-IR supercontinuum generation in an integrated liquid-core optical fiber filled with CS₂. *Opt. Mater. Exp.* **3**(9), 1358 (2013). <https://doi.org/10.1364/ome.3.001358>
25. Lanh, C.V., Van, T.H., Van, C.L., Borzycki, K., Khoa, D.X., Vu, T.Q., Trippenbach, M., Buczynski, R., Pniewski, J.: Supercontinuum generation in benzene-filled hollow-core fibers. *Opt. Eng.* **60**(11), 116109 (2021). <https://doi.org/10.1117/1.OE.60.11.116109>
26. Vieweg, M., Gissibl, T., Pricking, S., Kuhlmeier, B.T., Wu, D.C., Eggleton, B.J., Giessen, H.: Ultrafast nonlinear optofluidics in selectively liquid-filled photonic crystal fibers. *Opt. Express* **18**, 25232–25240 (2010). <https://doi.org/10.1364/OE.18.025232>
27. Cordier, M., Orioux, A., Gabet, R., Harle, T., Dubreuil, N., Diamanti, E., Delaye, P., Zaquin, I.: Liquid filled photonic crystal fiber: a flexible tool for fibered photon-pair generation. *Quantum Inf. Meas. (QIM)* (2017). <https://doi.org/10.1364/QIM.2017.QW3C.5>
28. Monfared, Y.E., Ponomarenko, S.A.: All-optical wavelength conversion using a liquid-filled photonic crystal fiber. 2017 Photonics North (PN). <https://doi.org/10.1109/PN.2017.8090575>
29. Ayyanar, N., Raja, R.V.J., Vigneswaran, D., Lakshmi, B., Sumathi, M., Porsezian, K.: Highly efficient compact temperature sensor using liquid infiltrated asymmetric dual elliptical core photonic crystal fiber. *Opt. Mater.* **64**, 574–582 (2017). <https://doi.org/10.1016/j.optmat.2017.01.011>
30. Vieweg, M., Pricking, S., Gissibl, T., Kartashov, Y., Torner, L., Giessen, H.: Tunable ultrafast nonlinear optofluidic coupler. *Opt. Lett.* **37**(6), 1058–1060 (2012). <https://doi.org/10.1364/OL.37.001058>
31. Chemnitz, M., Gaida, C., Gebhardt, M., Stutzki, F., Kobelke, J., Tünnermann, A., Limpert, J., Schmidt, M.A.: Carbon chloride-core fibers for soliton mediated supercontinuum generation. *Opt. Express* **26**(3), 3221–3235 (2018). <https://doi.org/10.1364/OE.26.003221>
32. Kato, T., Suetsugu, Y., Takagi, M., Sasaoka, E., Nishimura, M.: Measurement of the nonlinear refractive index in optical fiber by the cross-phase-modulation method with depolarized pump light. *Opt. Lett.* **20**(9), 988–990 (1995). <https://doi.org/10.1364/OL.20.000988>
33. D. M. Aviado.: Methyl chloroform and trichloroethylene in the environment, chapter 4, Boca Raton, 1st Edition (2017). ISBN: 9781351074506. <https://doi.org/10.1201/9781351074506>
34. Zhang, H., Chang, S., Yuan, J., Huang, D.: Supercontinuum generation in chloroform-filled photonic crystal fibers. *Optik* **121**(9), 783–787 (2010). <https://doi.org/10.1016/j.ijleo.2008.09.026>
35. Wang, C.-C., Li, W.-M., Li, N., Wang, W.-Q.: Numerical simulation of coherent visible-to-near-infrared supercontinuum generation in the CHCl₃-filled photonic crystal fiber with 1.06 μm pump pulses. *Opt. Laser Technol.* **88**, 215–221 (2017). <https://doi.org/10.1016/j.optlastec.2016.09.020>
36. Chu, V.L., Hoang, V.T., Long, V.C., Borzycki, K., Xuan, K.D., Quoc, V.T., Trippenbach, M., Buczyński, R., Pniewski, J.: Optimization of optical properties of photonic crystal fibers infiltrated with chloroform for supercontinuum generation. *Laser Phys.* **29**(7), 075107 (2019). <https://doi.org/10.1088/1555-6611/ab2115>
37. Islam, A.S.M.T.U., Ahmad, R., Hossen, I., Kabir, M.R., Bishwas, M.S., Faruque, O.: Wideband mid-infrared supercontinuum generation in chloroform filled suspended core fiber, 2020 2nd International Conference on Sustainable Technologies for Industry 4.0 (STI). <https://doi.org/10.1109/STI50764.2020.9350483>
38. Raj, G.J., Raja, R.V.J., Ganapathy, R.: Effect of chirp on supercontinuum generation in chloroform filled photonic crystal fiber with two zero dispersion wavelengths. 12th International Conference on Fiber Optics and Photonics. M4A.41 (2014). <https://doi.org/10.1364/PHOTONICS.2014.M4A.41>
39. Raja, R.V.J., Senthilnathan, K., Porsezian, K., Nakkeeran, K.: Efficient pulse compression using tapered photonic crystal fiber at 850 nm. *IEEE J. Quantum Electron.* (2010). <https://doi.org/10.1109/JQE.2010.2050865>
40. Dhasarathan, V., Sharafali, A., Tran, T.K., Mubashira Banu, E.P., Rajan, M.S.M.: Temperature independent photonic crystal fiber for spectroscopic and soliton pulse applications. *Optik* **271**, 170155 (2022). <https://doi.org/10.1016/j.ijleo.2022.170155>
41. Chemnitz, M., Gebhardt, M., Gaida, C., et al.: Hybrid soliton dynamics in liquid-core fibres. *Nat Commun* **8**, 42 (2017). <https://doi.org/10.1038/s41467-017-00033-5>
42. Mario, C., Christian, G., Martin, G., Fabian, S., Jens, K., Andreas, T., Jens, L., Markus, A.S.: Carbon chloride-core fibers for soliton mediated supercontinuum generation. *Opt. Express.* **26**(3), 3221–3235 (2018). <https://doi.org/10.1364/OE.26.003221>
43. Van, B.C., Hai, T.T., Thao, N.T., et al.: Experimental study of supercontinuum generation in water-filled-cladding photonic crystal fiber in visible and near-infrared region. *Opt. Quantum Electron.* **55**, 229 (2023). <https://doi.org/10.1007/s11082-022-04502-0>
44. Tan, C.Z.: Determination of refractive index of silica glass for infrared wavelengths by IR spectroscopy. *J. Non-Cryst. Solids* **223**(1–2), 158–163 (1998). [https://doi.org/10.1016/s0022-3093\(97\)00438-9](https://doi.org/10.1016/s0022-3093(97)00438-9)
45. Zhu, Z., Brown, T.G.: Full-vectorial finite-difference analysis of microstructured optical fibers. *Opt. Express* **10**, 853–864 (2002). <https://doi.org/10.1364/OE.10.000853>
46. Saitoh, K., Florous, N.J., Koshihara, M.: Theoretical realization of holey fiber with flat chromatic dispersion and large mode area: an intriguing defected approach. *Opt. Lett.* **31**(1), 26–28 (2006). <https://doi.org/10.1364/OL.31.000026>
47. Alam, M.Z., Tahmid, M.I., Mouna, S.T., Islam, M.A., Alam, M.S.: Design of a novel star type photonic crystal fiber for mid-infrared supercontinuum generation. *Opt. Commun.* **500**, 127322 (2021). <https://doi.org/10.1016/j.optcom.2021.127322>
48. Hossain, M.M., Ahsan, M.S., Sikder, N., Rahaman, M.E., Al-Mamun Bulbul, A., Mondal, H.S.: High birefringence and broadband dispersion compensation photonic crystal fiber. *J. Opt. Commun.* (2012). <https://doi.org/10.1515/joc-2020-0140>
49. Rahaman, M.E., Hossain, M.M., Mondal, H.S., Saha, R., Munta-seer, A.S.: Theoretical analysis of large negative dispersion

- photonic crystal fiber with small confinement loss. *Appl. Opt.* **59**(28), 8925–8931 (2020). <https://doi.org/10.1364/AO.397420>
50. Zeng, F., and Li, B.: Theoretical investigation on the propagation and super-continuum generation of an ultra-short pulse in a highly nonlinear fiber. *Proceedings 10619, 2017 International Conference on Optical Instruments and Technology: Advanced Laser Technology and Applications; 106190Z* (2018). <https://doi.org/10.1117/12.2296367>
 51. Willer, U., Saraji, M., Khorsandi, A., Geiser, P., Schade, W.: Near- and mid-infrared laser monitoring of industrial processes, environment and security applications. *Opt. Lasers Eng.* **44**(7), 699–710 (2006). <https://doi.org/10.1016/j.optlaseng.2005.04.015>
 52. Kedenburg, S., Vieweg, M., Gissibl, T., Giessen, H.: Linear refractive index and absorption measurements of nonlinear optical liquids in the visible and near-infrared spectral region. *Opt. Mater. Express* **2**(11), 1588–1611 (2012). <https://doi.org/10.1364/OME.2.001588>
 53. Kalantari, M., Karimkhani, A., Saghaei, H.: Ultra-Wide mid-IR supercontinuum generation in As_2S_3 photonic crystal fiber by rods filling technique. *Optik* **158**, 142–151 (2018). <https://doi.org/10.1016/j.ijleo.2017.12.014>
 54. Guo, Y., Jafari, Z., Xu, L., Bao, C., Liao, P., Li, G., Agarwal, A.M., Kimerling, L.C., Michel, J., Willner, A.E., Zhang, L.: Ultra-flat dispersion in an integrated waveguide with five and six zero-dispersion wavelengths for mid-infrared photonics. *Photonics Res.* **7**(11), 1279–1286 (2019). <https://doi.org/10.1364/PRJ.7.001279>
 55. Wang, Y., Fang, Y., Geng, W., Jiang, J., Wang, Z., Zhang, H., Bao, C., Huang, H., Ren, Y., Pan, Z., Yue, Y.: Beyond two-octave coherent OAM supercontinuum generation in air-core As_2S_3 ring fiber. *IEEE Access* **8**, 96543–96549 (2020). <https://doi.org/10.1109/ACCESS.2020.2996666>
 56. Agrawal, G.P.: *Nonlinear Fiber Optics* (5th edition). Academic Press, Elsevier. (2013). ISBN: 978-0-12-397023-7. <https://doi.org/10.1016/C2011-0-00045-5>
 57. Kajla, A., Gupta, S.: Evaluation of confinement loss of different photonic crystal fibers on the basis of varying the size and shape of holes. *Int. J. Eng. Res. Technol. (IJERT)* **3**(2), 1521–1525 (2014)
 58. Zhao, P., Reichert, M., Benis, S., Hagan, D.J., Stryland, E.W.V.: Temporal and polarization dependence of the nonlinear optical response of solvents. *Optica* **5**(5), 583–594 (2018). <https://doi.org/10.1364/OPTICA.5.000583>
 59. Finot, C., Kibler, B., Provost, L., Wabnitz, S.: Beneficial impact of wave-breaking for coherent continuum formation in normally dispersive nonlinear fibers. *J. Opt. Soc. Am. B* **25**, 1938–1948 (2008). <https://doi.org/10.1364/JOSAB.25.001938>
 60. Hooper, L.E., Mosley, P.J., Muir, A.C., Wadsworth, W.J., Knight, J.C.: Coherent supercontinuum generation in photonic crystal fiber with all-normal group velocity dispersion. *Opt. Express* **19**(6), 4902–4907 (2011). <https://doi.org/10.1364/OE.19.004902>
 61. Amin, R., Abdulrazak, L.F., Tahhan, S.R., Mohammadd, N., Ahmed, K., Bui, F.M., Ibrahim, S.M.: Tellurite glass based optical fiber for the investigation of supercontinuum generation and nonlinear properties. *Phys. Scr.* **97**(3), 03007 (2022). <https://doi.org/10.1088/1402-4896/ac5359>

Publisher's Note Springer Nature remains neutral with regard to jurisdictional claims in published maps and institutional affiliations.

Springer Nature or its licensor (e.g. a society or other partner) holds exclusive rights to this article under a publishing agreement with the author(s) or other rightsholder(s); author self-archiving of the accepted manuscript version of this article is solely governed by the terms of such publishing agreement and applicable law.